



# Microstructural evolution in adiabatic shear band in the ultrafine-grained austenitic stainless steel processed by multi-axial compression



Bingfeng Wang <sup>a,b,c,d,\*</sup>, Zhaolin Liu <sup>a</sup>, Bin Wang <sup>b,c</sup>, Shiteng Zhao <sup>b,c</sup>, Jieying Sun <sup>a</sup>

<sup>a</sup> School of Materials Science and Engineering, Central South University, Changsha 410083, Hunan, People's Republic of China

<sup>b</sup> Department of Mechanical and Aerospace Engineering, University of California, San Diego, CA 92093, United States

<sup>c</sup> Department of Nanoengineering, University of California, San Diego, CA 92093, United States

<sup>d</sup> Key Lab of Nonferrous Materials, Ministry of Education, Central South University, Changsha 410083, Hunan, People's Republic of China

## ARTICLE INFO

### Article history:

Received 7 March 2014

Received in revised form

20 May 2014

Accepted 28 May 2014

Available online 3 June 2014

### Keywords:

Steels

Shear bands

Electron microscopy

Recrystallization

EBSD

## ABSTRACT

Adiabatic shear bands play the most important role in the deformation and failure of high strength AISI 201 austenitic stainless steel. The microstructure and microtexture of the adiabatic shear band in ultrafine-grained stainless steel are investigated by means of optical microscopy, TEM and EBSD. The shear bands can be generated at about 54  $\mu$ s after the true flow stress reaches the peak value of about 1135 MPa. The width of the shear bands is about 9  $\mu$ m, and the grains sizes 50–200 nm in the boundary of the shear band are elongated along the shear direction; the grain subdivision on approaching the shear band can be observed, and the core of the shear band consists of recrystallized equiaxed grains (sizes 30–80 nm) with new microtextures and the ultrafine grains with deformed microtextures and with high dislocation density. The grain boundaries in the adiabatic shear band are geometrical necessary boundaries with high-angles. The calculated temperature in the shear band is estimated to reach 0.58  $T_m$  (968 K). It takes 7  $\mu$ s for the shear band to cool down from 968 K to the room temperature when the shear localization ceases, and the cooling strain rate is calculated as high as  $9.6 \times 10^7$  K/s. Kinetic calculations indicate that during the deformation process, the recrystallized nanosized grains can be formed in the shear band by way of the subgrain boundaries rotation when the subgrains' sizes are lower than 80 nm or the temperature in the shear band is higher than 0.5  $T_m$  (834 K), and they do not undergo significant growth by grain boundary migration at the cooling stage. These results indicate that the microstructure development within shear band is controlled by both dynamic recovery and rotational dynamic recrystallization.

© 2014 Elsevier B.V. All rights reserved.

## 1. Introduction

Adiabatic shear band is a distinct characteristic of highly localized deformation occurring in materials when subjected to dynamic loading. This phenomenon is often an important precursor for dynamic failure and has been widely studied for many years [1–4]. The microstructure within shear bands observed in post-deformation observations provides some information to understand the thermal-mechanical evolution during shear localization. It has been found that the microstructure of adiabatic shear bands is different in various materials. Adiabatic shear bands have been classified into the deformed band with elongated microstructure along the shear

direction and the transformed band. The white etching shear bands in steel attributed to steel's austenite phase quenched into martensite phase at the high temperatures [1,3,5]. It is now recognized that the fine substructure may not in fact come from this phase transformation but instead from a wide range of mechanisms such as dynamic recovery [6], recrystallization [7–9], and amorphization [3].

Recently, the new generation ultrafine-grained steel project has been conducted in a few countries. The main features of the new generation steels are high purity, ultrafine grains and high homogeneous properties. These steels have higher strength, longer service lifetime and more economical compared to conventional steels [10–12]. Most of the published research work on ultrafine-grained steel has been carried out under quasi-static loading; however, there are few reports on the ultrafine-grained steel under dynamic loading, especially the study of the adiabatic shear bands in it.

In the present work, we investigate the localized plastic deformation of ultrafine-grained AISI 201 stainless steel processed by

\* Corresponding author at: University of California, San Diego, 9500 Gilman Drive, La Jolla, CA 92093, United States. Tel.: +1 858 900 6320; fax: +1 858 534 7078.  
E-mail address: [biw009@ucsd.edu](mailto:biw009@ucsd.edu) (B. Wang).

multi-axial compression under controlled dynamic compressive loading. The aims of this paper are (1) to capture the mechanical response of the ultrafine-grained AISI 201 stainless steel under controlled dynamic loading, (2) to characterize the microstructure and microtexture in the adiabatic shear band, and (3) to discuss the microstructure evolution mechanism in the shear band.

## 2. Experimental

The material used in this study is the AISI 201 stainless steel with chemical composition (wt%) 0.15% C, 0.75% Si, 5.5% Mn, 16% Cr, 0.25% N, 0.06% P, 1% Ni, 0.03% S, and balance iron. The ultrafine-grained stainless steel was prepared by the multi-axial compression carried out at 973 K and at the strain rate of  $1.5 \times 10^{-2} \text{ s}^{-1}$ , using a rectangular sample with dimensions of  $20 \text{ mm} \times 16 \text{ mm} \times 13 \text{ mm}$ . Successive uniaxial compression of  $\varepsilon = -0.4$  was applied to the longest side at each strain step and the accumulative strain ( $\Sigma\Delta\varepsilon$ ) was up to 2.8. The details of the multi-axial compression are described elsewhere [13]. The grain sizes in the specimen are about 5  $\mu\text{m}$  (Fig. 1).

Hat-shaped specimens were prepared parallel to the last compression axis for the dynamic loading. The hat-shaped specimens, originally mentioned by Meyer and Marwaring [14], as shown in Fig. 2, were used to produce well-controlled shear bands at high strain rates. The dynamic compression of hat-shaped specimens was carried out using a split Hopkinson pressure bar at 293 K, and the stopper rings with different thicknesses were used to control the deformation.

After dynamic compression, the samples were cut, ground and polished along the compression axis. Electro-etching was performed with an electro-etchant solution of 10% oxalic acid and 90% water at 6 V. The optical micrograph of the adiabatic shear bands was performed with POLYVAR-MET. The transmission

electron microscopy (TEM) samples were thinned and polished to a thin foil and were cut into 3 mm disks. A Gatan dimpler was used to locate the regions to be thinned on the paths of shear bands. Ion milling was completed on a Gantan precision ion polishing system to ensure perforation exactly on the shear bands. The TEM observations were carried out with a Tecnai G<sup>2</sup> F20 transmission electron microscope operated at 200 kV. A high-resolution Helios Nanolab 600i scanning electron microscope operated at 20 kV was used to characterize the microtexture evolution and grain boundaries characterization within the shear section. The 0.05  $\mu\text{m}$  step size and higher magnification were employed. Electron backscattered diffraction (EBSD) data was analyzed using commercially available TSL-OIM software. From the measured orientations, the orientation distribution functions are calculated. The  $\varphi_1$ ,  $\Phi$  and  $\varphi_2$  angles are the conventional Euler angles. The reference system is taken so that the shear direction (SD) and the shear plane normal (SPN) are approximately parallel to  $x$ - and  $y$ -axes of the figure. For convenience, two sections of  $\varphi_2=0^\circ$ ,  $45^\circ$  in the orientation distribution functions are used to illustrate texture components.

## 3. Results and discussion

### 3.1. Mechanical response of the specimen

When the specimen was loaded by the split Hopkinson pressure bar, the force applied to the shear band was calculated from data collected by the strain gauges on the incident and transmitted bars. The shear stress, strain rate, nominal strain and the true stress can be calculated by the following equations [15]:

$$\tau = \frac{E_0 A_s \varepsilon_i(t)}{\pi h(d_i + d_e/2)} \quad (1)$$

$$\dot{\gamma} = \frac{2C_0[(\varepsilon_i(t) - \varepsilon_t(t)]}{s} \quad (2)$$

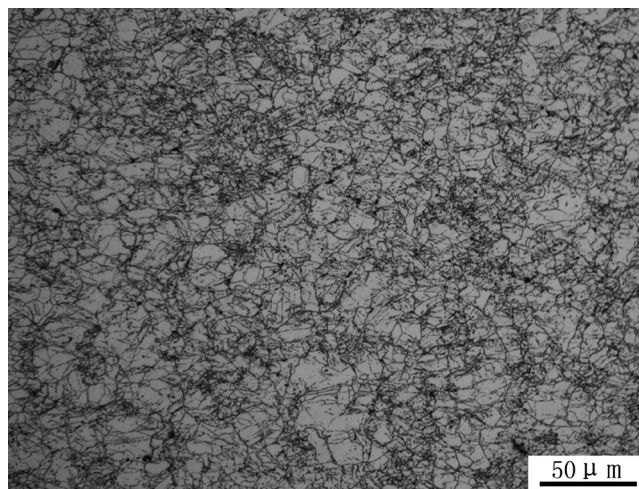
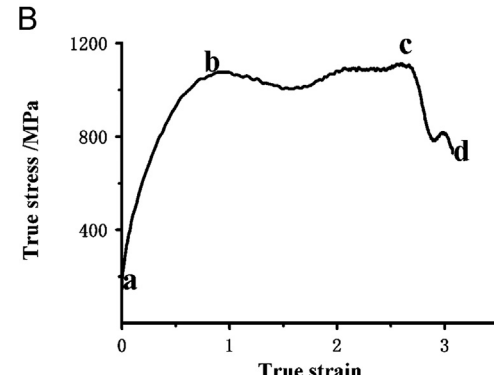
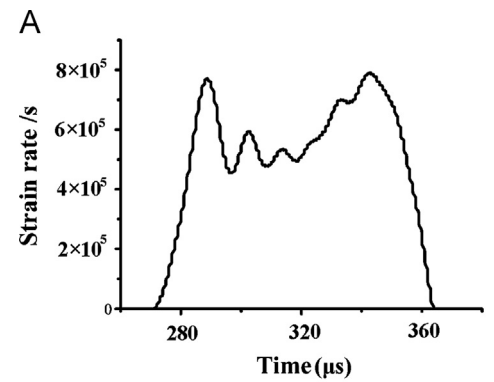


Fig. 1. Initial microstructure of specimen with small grain size.

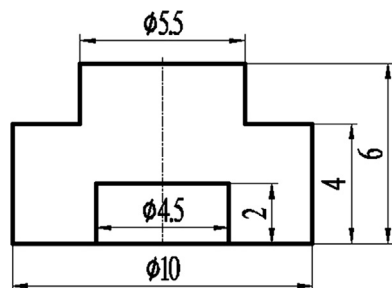


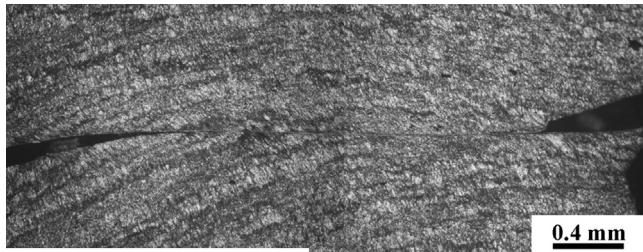
Fig. 2. Schematic diagram of the hat-shaped specimen. (Dimensions in mm.)

Fig. 3. Dynamic responses of specimen at high strain rate, (A) strain rate-time curves, and (B) true stress-true strain curves.

$$\gamma = \frac{2C_0 \int_0^t [(\varepsilon_i(t) - \varepsilon_t(t))] dt}{s} \quad (3)$$

$$\sigma = 2\tau \quad (4)$$

where  $E_0$  and  $C_0$  are the elastic modulus and elastic wave speed,  $h$  and  $s$  are the thickness of the shear section and the width of the shear band,  $d_i$  and  $d_e$  are the diameter of the hat and the base hole,



**Fig. 4.** Optical micrograph of an adiabatic shear band.

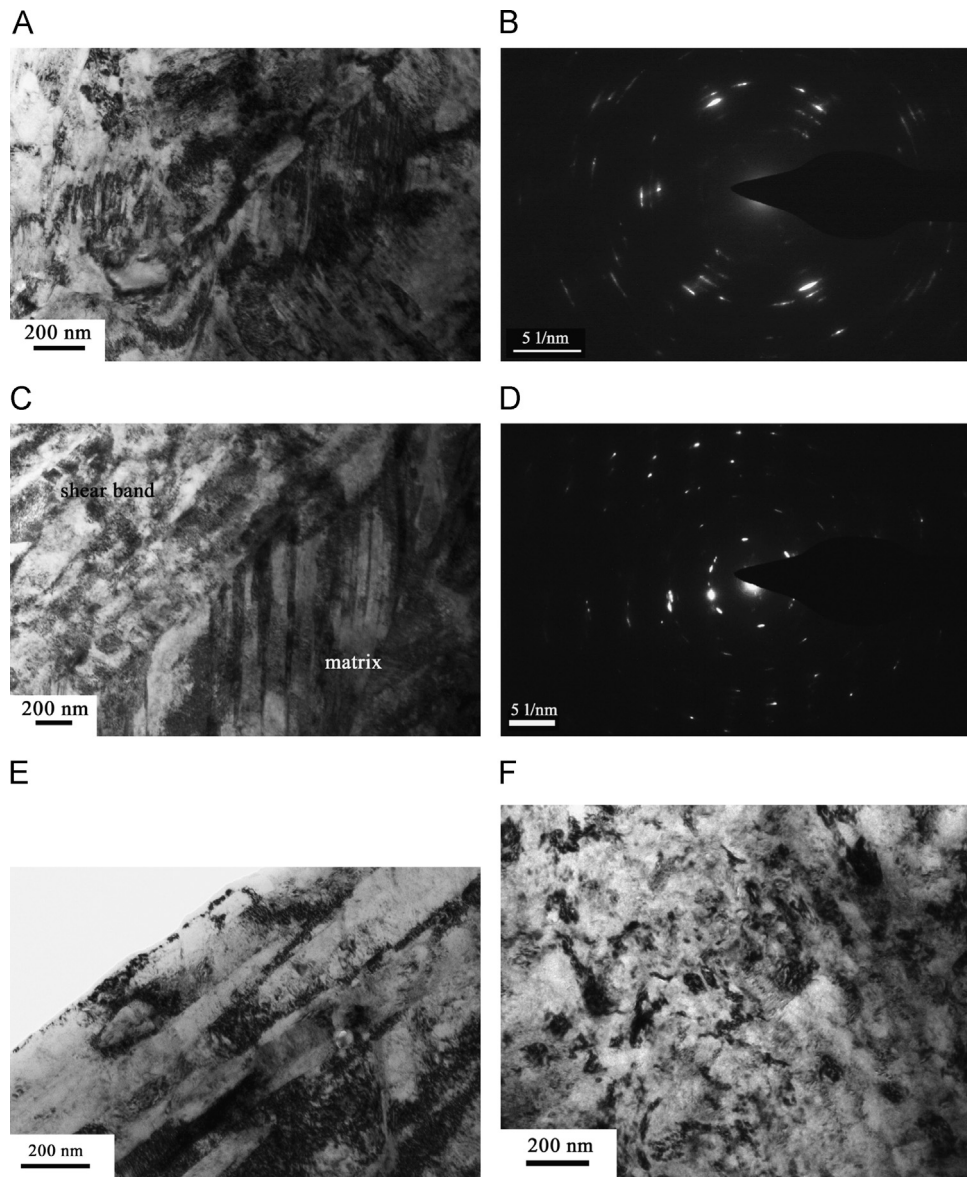


**Fig. 5.** Transmission electron micrographs of the specimen, (A) the grains in the matrix, (B) corresponding selected area diffraction pattern in the matrix, (C) the boundary between the matrix and the shear band, (D) the selected area diffraction pattern of the lamellar pearlite in the matrix in (C), (E) the elongated grains in the boundary, and (F) the grains in the center zone.

and  $\varepsilon_r(t)$  and  $\varepsilon_t(t)$  are the experimentally measured strain of reflected and transmitted stress pulse on the Hopkinson bars, respectively.

Culver [16] introduced a simple relation between the true strain ( $\varepsilon$ ) and the shear strain expressed as Eq. (5).

$$\varepsilon = \ln \sqrt{1 + \gamma + \frac{\gamma^2}{2}} \quad (5)$$

The true strain–stress curve of hat-shaped sample tested by the split Hopkinson pressure bar is shown in Fig. 3. The strain rate during shear deformation can be calculated from the relationship between voltage pulse and loading time at the controlled dynamic testing and Eq. (2), as shown in Fig. 3A. Thus, the specimen was tested at the strain rate about  $4.8 \times 10^5 \text{ s}^{-1}$ . The adiabatic shearing deformation starts from the first peak value of the strain rate to the last loading peak [15], and the whole process lasts about 54  $\mu\text{s}$  (Fig. 3A). There are three stages proceeded during the dynamic loading (Fig. 3B). In the first stage (A–B), the true flow stress increases with the true strain sharply due to the strain hardening and strain rate hardening, and the true flow stress reaches the

maximum value of about 1135 MPa at the first vibration peak. In the second stage (B–C), the true flow stress fluctuates in a small area with an increase of the true strain to 2.65 as a result of the rough balance of the thermal softening and the strain hardening and strain rate hardening. In the last stage (C–D), the true stress sharply decreases as the strain increases for the reason that the effect of the thermal softening is obviously larger than the effect of the strain hardening and the strain rate hardening during this process. The thermoviscoplastic instability of the material occurs in this stage, and an adiabatic shear band is generated in the specimen.

### 3.2. Microstructure within a shear band

**Fig. 4** shows the optical micrograph of an adiabatic shear band in the ultrafine-grained AISI 201 stainless steel. It can be seen that the shear band is a long and straight band with width about 9 μm distinguished from the matrix by obvious boundaries, and the grains in the transition zone between the center of the shear band and the matrix are elongated along the shear direction.

The boundary between an adiabatic shear band and its outside area provides valuable information about the formation and development of the substructures within a shear band. The grains in the matrix consist of austenitic with face centered cubic crystal structures and lamellar pearlite, as shown in **Fig. 5A–D**. The lamellar pearlite may be caused by partial segregation of materials. **Fig. 5C** shows a shear band's boundary separating the shear localized region inside the shear band from the heavily deformed region outside the shear band. It can be seen that the grains in the boundary of the shear band are highly elongated along the shear direction and form the elongated cell structures (50–200 nm in width) with high dislocation density due to the strong shear deformation upon the shear band, and elongated cell structures break up into several subgrains with little misorientations (**Fig. 5E**). **Fig. 5C** also shows that the shear band

intersects with the matrix. **Fig. 5F** illustrates the microstructure in the center of the shear band. It consists of a few nanosized equiaxed grains of diameters varying from 30 nm to 80 nm with low dislocation density and some largely deformed grains with blurred grain boundaries. Therefore, the recrystallization has not occurred universally in the band center, and the initial deformed substructures have been partly preserved.

### 3.3. Microtexture measurement within a shear band

The EBSD technique is used to measure microstructure and microtexture in the matrix and the adiabatic shear band. The high-angle boundaries shown (**Figs. 6 and 7A**) as black lines are the grain boundaries with misorientations larger than 15°, and the low-angle boundaries are indexed by white lines. It can be seen that the matrix consists of ultrafine equiaxed grains and deformed elongated grains.

**Fig. 7** shows the EBSD micrographs of the center in the shear band. The black regions of the orientation imaging microscopy map are areas where no orientation data can be acquired due to larger density of dislocations, or a very fine microstructure with a smaller scale exceeding the resolution limit of EBSD (ca. 0.12 μm) (**Fig. 7A**). It is found that misorientations across grain boundaries are larger than 20°, and peaked at 40–55°, which suggests that the grain boundaries are geometrical-necessary boundaries (**Fig. 7C**). Therefore, ultrafine equiaxed grains in the shear band possess high percentage of high-angle boundaries and geometrical-necessary boundaries developed with an aim of accommodating the imposed shear strain.

Furthermore, the image quality index can qualitatively reflect the defect density and/or lattice strain [17]. Dislocation density causes the change of the image quality index of the EBSD measured. Many dark grains emerged in the center of the shear band, and some light regions are also found (**Fig. 7B**). Thus, some ultrafine grains with low dislocation density are formed in the shear band. The calculated orientation distribution function maps indicate that some grains orientation distribution peaks in the matrix remain in the core of the shear band, and some new grains orientation distribution peaks are also generated such as (0°, 49°, 0°) and (90°, 90°, 45°), as shown in **Figs. 6B and 7D**. Therefore, ultrafine equiaxed grains with low dislocation density coexist with deformed grains with high dislocation density in the center of the shear band.

### 3.4. Calculation of temperature in a shear band

At high strain rates ( $> 10^3 \text{ s}^{-1}$ ), the deformation process is extremely fast and can be considered as an adiabatic process. Temperature rise in an adiabatic shear band associated with the deformation plays a significant role in the study of microstructure mechanism and is calculated by the following equation [3,18]:

$$T = T_0 + \Delta T = T_0 + \frac{\eta}{\rho C_v} \int_{\epsilon_s}^{\epsilon_e} \sigma d\epsilon \quad (6)$$

where  $T_0$  is the initial deformation temperature,  $\rho$  is the mass density,  $C_v$  is the heat capacity,  $\epsilon$  is the strain,  $\sigma$  is the stress and  $\eta$  is the fraction of plastic energy converted to heat, commonly  $\eta=0.9$ . For stainless steel,  $\rho$  is 7.9 g/cm<sup>3</sup>,  $C_v$  is 500 J/kg, and  $T_0$  is 293 K [19].

Substituting the dynamic response data in the shear band during plastic deformation shown in **Fig. 3** into Eq. (6), the adiabatic temperature rise can be estimated as follows:

$$T = T_0 + \Delta T = T_0 + \frac{\eta}{\rho C_v} \int_{\epsilon_s}^{\epsilon_e} \sigma d\epsilon = T_0 + \frac{\eta}{\rho C_v} \sum_{i=1}^n S_i \quad (7)$$

where  $S_i$  is the deformation energy per volume. The dynamic mechanical response data in the shear band can be divided into a large number (n) of continuous blocks with strain increment  $\Delta\epsilon_i$ .

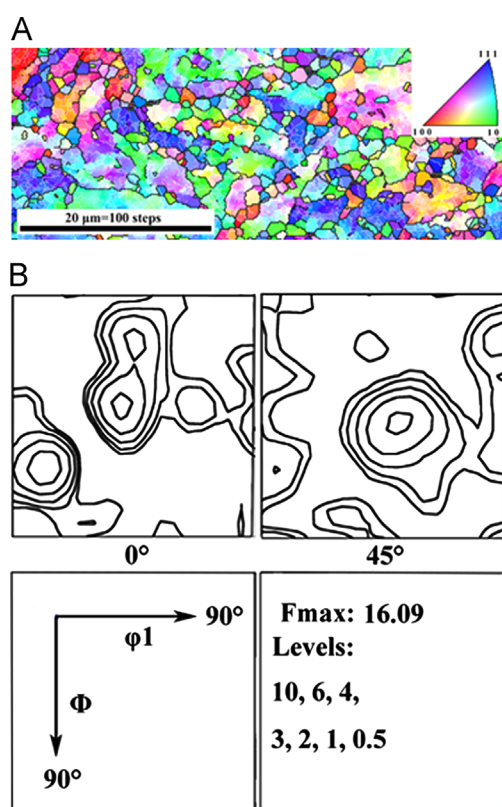


**Fig. 6.** EBSD micrographs taken from in regions close to the shear band, (A) orientation imaging micrograph map, and (B) orientation distribution function map.

And the area of the each block can be calculated as the following expression:

$$S_i = \frac{\Delta \varepsilon_i \times (\sigma_i + \sigma_{(i+1)})}{2} (i = 1, 2, 3 \dots) \quad (8)$$

It can be noticed that the maximum temperature in the forced localized shear zone is about 968 K ( $T/T_m=0.58$ ). Therefore, the temperature rise in the shear band is high enough to meet the needs of recrystallization for AISI 201 stainless steel (0.4–0.5  $T_m$ ).

During the cooling process, the classical Fourier heat conduction equation is used to estimate the temperature within the

shear zone [20].

$$\rho C_v \frac{\partial T}{\partial t} = K_0 \nabla^2 T + \tau \dot{y} \quad (9)$$

Since the shear band is very narrow and axially symmetric, a reasonable estimate can be obtained using one dimensional calculation which considers a small shear band in an infinite medium. Assuming a constant rate of heat generation in the thin shearing zone, the solution of the heat equation can be reduced to the following expression [20]:

$$T(x, t) = \frac{2d_s(T_{max} - T_0)}{\sqrt{4\pi m t}} e^{-(x - R_i)^2 / 4mt} (R_i - d_s < x < R_i + d_s) \quad (10)$$

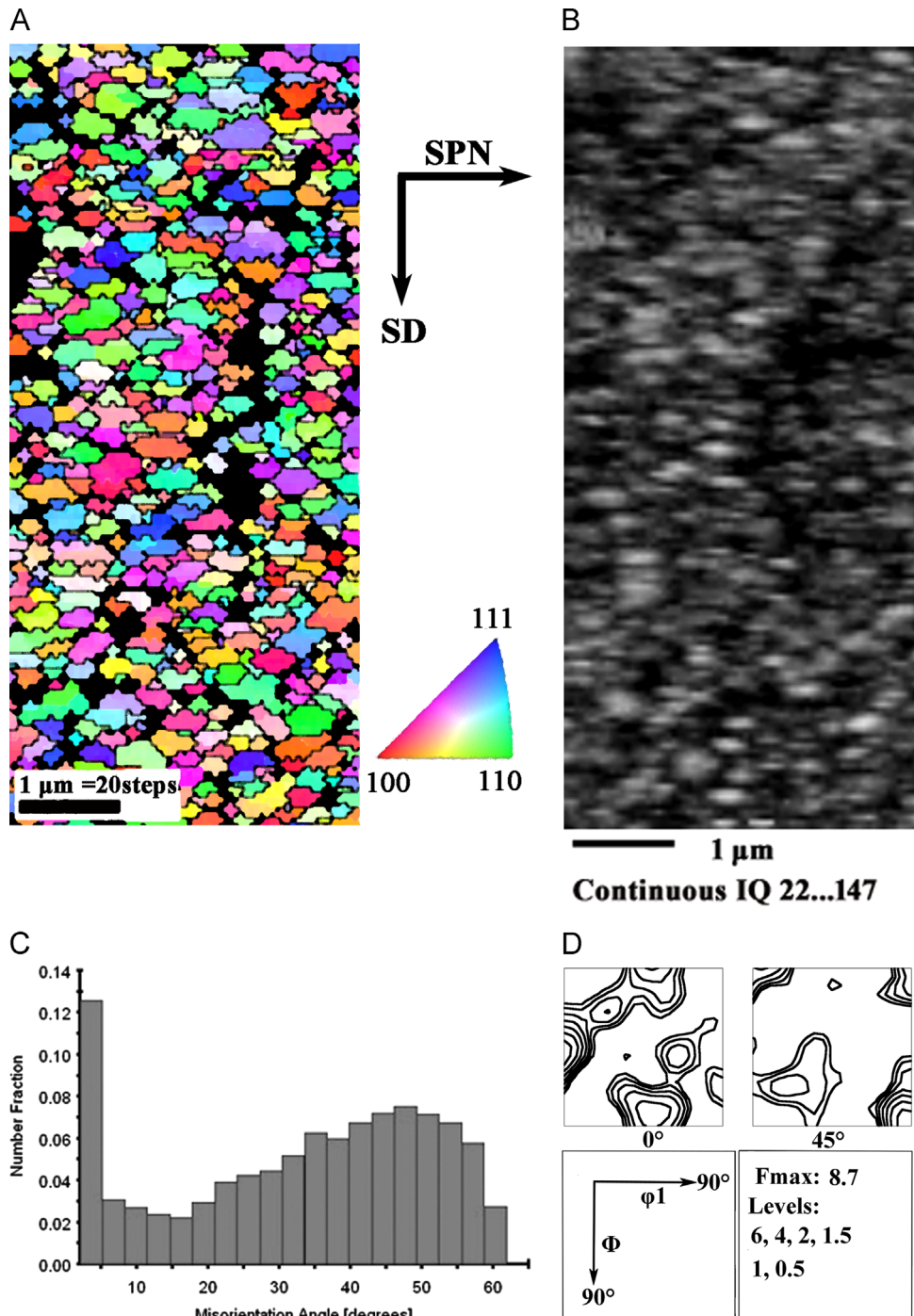


**Fig. 7.** EBSD micrographs taken from the shear band center, (A) orientation imaging micrograph map, and (B) imaging quality map, and (C) misorientation angle map, and (D) orientation distribution function map.

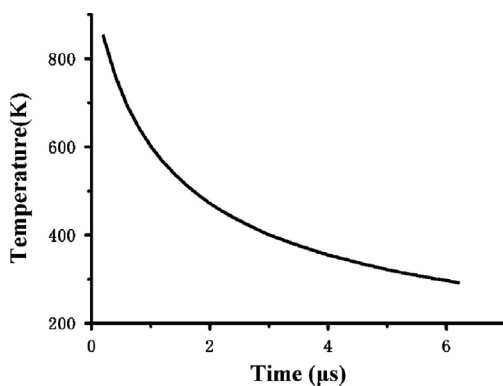


Fig. 8. Calculated temperature in the shear band drop as a function of time.

where  $m$  is a material constant ( $m=K_0/(\rho C_v)$ ), and  $K_0$  is the thermal conductivity of stainless steel,  $T_{max}$  is the maximum temperature within the shear band after the deformation, and  $d_s$  and  $R_i$  are the half-width of shear bands and the distance from the center of shear band to the center of the hat-shaped specimen, respectively. The parameters used in Eq. (10) are the following.  $K_0$  is 20 W/(m K) [21],  $T_{max}$  is 968 K,  $T_0$  is 293 K,  $d_s$  is 4.5 μm,  $R_i$  is 5 mm, and  $x$  is taken as the 5 mm, which means to analyze temperature cooling process in the core of the shear band.

The calculated temperature during the cooling process at the center of the shear band is shown in Fig. 8. It takes 7 μs for the shear band to cool down from 968 K to ambient temperature when the shear localization ceases. The cooling rate is as high as  $9.6 \times 10^7$  K/s. Therefore, in such a short time, the high-temperature microstructure in the shear band should be preserved.

### 3.5. Mechanism of microstructure evolution in a shear band

The above analysis of the microstructure and microtexture of the adiabatic shear band in UFG AISI 201 stainless steel indicates that the nanosized equiaxed grains with new microtextures and ultrafine grains with high dislocation density coexist in the center of the shear band. The thermodynamic calculation results suggest that the temperature rise in the shear band is high enough to meet the needs of recrystallization of AISI 201 stainless steel. Therefore, the grain refinement of the shear band in ultrafine-grained AISI 201 stainless steel is attributed to the results of both the dynamic recovery and the dynamic recrystallization.

The high percentages of the high-angle boundaries and the geometrical-necessary boundaries suggest that rotational dynamic recrystallization mechanism may be appropriate to understand the formation of the new nanosized equiaxed grains in the present work.

According to the rotational dynamic recrystallization mechanism [3,22–24], the process of fragmentized subgrain boundaries should rotate 30° to form high-angle boundaries recrystallized grains. The time required for the rotation process is described as the following equation [3,24]:

$$t = \frac{L_1 k T f(\theta)}{4\delta\eta D} = \frac{L_1 k T f(\theta)}{4\delta\eta D_0 \exp(-Q_b/RT)} \quad (11)$$

where  $L_1$  is the average size of the subgrains diameter,  $\delta$  denotes the grain boundary thickness,  $\eta$  is the grain boundary energy,  $D_0$  is a constant related to grain boundary diffusion,  $Q_b$  represents the activation energy of grain boundary diffusion. For AISI 201 stainless steel,  $L_1$  is 30–80 nm,  $\delta$  is about 0.5 nm,  $k$  is  $1.38 \times 10^{-23}$  J/K,  $R$  is 8.314 J/mol,  $\eta$  is 0.625 J/m<sup>2</sup>,  $D_0$  is  $3.7 \times 10^{-5}$  m<sup>2</sup>/s, and  $Q_b$  is

167 kJ/mol [3].  $f(\theta)$  can be expressed as

$$f(\theta) = \frac{3 \tan \theta - 2 \cos \theta}{3 - 6 \sin \theta} - \frac{4\sqrt{3}}{9} \ln \frac{2 + \sqrt{3}}{2 - \sqrt{3}} + \frac{4\sqrt{3}}{9} \ln \frac{\tan(\theta/2) - 2 - \sqrt{3}}{\tan(\theta/2) - 2 + \sqrt{3}} + \frac{2}{3} \quad (12)$$

where  $\theta$  is from 0° to nearly 30°. The maximum temperature within the shear band is calculated about 968 K and the whole time for the dynamic loading lasts for 54 μs. The kinetic curves for the rotational dynamic recrystallization mechanism in the present work can be obtained by substituting the parameters into Eqs. (11) and (12), as shown in Fig. 9. The temperature is varied from 0.45  $T_m$  to 0.58  $T_m$  for a subgrain size of 80 nm (Fig. 9A); and the subgrain size  $L_1$  is varied from 80 nm to 200 nm at  $T=0.58 T_m$  (Fig. 9B). The results show that the grain-boundary rotation is accomplished within 20 μs when the subgrain size  $L_1$  varies from 80 nm to 200 nm at  $T=0.58 T_m$  (968 K), and larger subgrain size and lower temperature result in more time being needed for recrystallization. It is worth noting that the deformation time (54 μs) is enough for the formation of the ultrafine grains in the shear band by the way of the subgrains boundaries rotation. Thus,

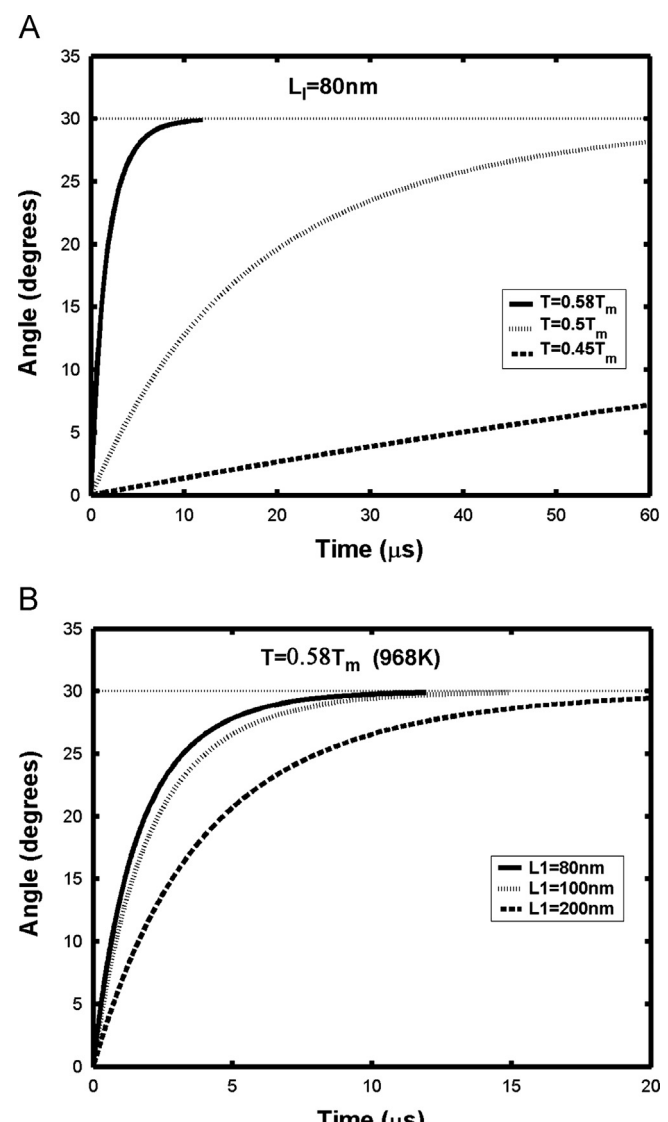


Fig. 9. Angle of rotation of subgrains boundary in stainless steel as a function of needed time for (A) different temperatures for  $L_1=80$  nm, and (B) different subgrains size at  $0.58 T_m$ .

the rotational dynamic recrystallization mechanism can take effect on the formation of the new nanosized equiaxed grains in the present work. At the same time, we note that the subgrains with sizes of 80 nm cannot finish the process of rotational recrystallization within the loading time until the temperature within an adiabatic shear band is above  $0.5 T_m$  (834 K) (Fig. 9A). Guduru [25], Li [26] and Yang [27] studied the temperature distribution within the shear band by experimentation and computer simulation. Their results indicated that the temperature distribution was non-uniform along the shear band. It was decreased from the center to the boundary, and the hot spots were located within the center of the shear band, leading to the shear strains fluctuate along the shear direction. If the shear strains in some regions within the shear band are small, the temperature in these regions may be less than  $0.5 T_m$  (834 K), and then the deformed subgrains in these regions cannot finish the process of rotational recrystallization and preserve the deformation states, that is, the dynamic recovery and the dynamic recrystallization can coexist in the shear band.

During the cooling stage, the rotational dynamic recrystallization mechanism cannot take effect due to the absence of mechanical assistance, and the grain growth must be in the way of grain migration. Migrational recrystallization mechanisms based on diffusion are tightly related to temperature and surely occur when the temperature becomes very high. According to the conventional migrational grain growth theory, a continuous grain growth can be illustrated as follows [28]:

$$L^n - L_0^n = K(T)t \quad (13)$$

where  $L$  is the final mean grain size,  $L_0$  is the initial grain size,  $n$  is the grain growth exponent, and  $K(T)$  is a temperature dependent constant. The parameter  $K(T)$  is defined as follows:

$$K(T) = m_0 \exp\left(-\frac{Q}{RT}\right) \quad (14)$$

where  $m_0$  and  $Q$  are the pre-exponential coefficient and the activation energy for grain growth, respectively. The maximum temperature ( $T$ ) and possible cooling time ( $t$ ) and possible initial grain size ( $L$ ) for the ultrafine-grained AISI 201 stainless steel are 968 K, 7  $\mu$ s and 80 nm, respectively. For steel [29],  $Q=177$  kJ/mol,  $m_0=21$ ,  $n=1.7$ , and  $R=8.314$  J/(mol k). Then, the calculated  $K(T)$  and  $L$  are  $5.8926 \times 10^{-9}$  and 82.234 nm, respectively. Thus, it is concluded that ultrafine grains formed during the deformation process cannot significantly grow up at the cooling stage.

#### 4. Conclusions

After shear deformation of about 54  $\mu$ s, the shear band with the width about 9  $\mu$ m is generated in an ultrafine-grained AISI 201 stainless steel processed by multi-axial compression under controlled dynamic loads. The unstable shear deformation of the alloy emerged after the true flow stress reaches the first vibration peak 1135 MPa. Microstructure and microtexture in an adiabatic shear band in an ultrafine-grained AISI 201 stainless steel under controlled dynamic loads are characterized in this paper. An adiabatic shear band is found with the width of about 9  $\mu$ m, and has obvious boundary between the shear band and the matrix. The grains in the boundary of the shear band are highly elongated cell structures of width 50–200 nm and they would split into several subgrains with small misorientations along the shear direction. The core of the shear band consists of the nanosized equiaxed grains with new microtextures and ultrafine grains with deformed microtextures and high dislocation density. The grains in the shear band possess high percentage of the high-angle boundaries and

the geometrical-necessary boundaries developed with an aim of accommodating the imposed shear strain.

Thermal and mechanical evolutions during the formation of shear band are described by combining dynamic response data and the quantitative calculation of adiabatic temperature rise and drop. The temperature within the shear band rises from 293 K to 968 K within 54  $\mu$ s during shear deformation. Then, it takes 7  $\mu$ s for the shear band to cool down from 968 K to the room temperature when the shear localization ceases, and the cooling strain rate is calculated as high as  $9.6 \times 10^7$  K/s. The kinetic calculations reveal that the recrystallized nanosized grains can be formed in the shear band when the subgrain's size is lower than 80 nm or the temperature in the shear band is higher than  $0.5 T_m$  (834 K) during the deformation process and they do not undergo significant growth by grain boundary migration at the cooling stage. Due to the inhomogeneous temperature distribution in the shear band, some ultrafine grains with recovery characteristics are also formed. Therefore, dynamic recovery and rotational boundaries dynamic recrystallization take effect on the formation of microstructure in the adiabatic shear band in the ultrafine-grained AISI 201 stainless steel processed by multi-axial compression.

#### Acknowledgment

This work was financially supported by Project supported by Hunan Provincial Natural Science Foundation of China (No. 12JJ2028), by Major Science and Technology Project of Hunan in China (No. 2010F51004), by a scholarship from the China Scholarship Council (No. 201308430093) and by the Freedom Explore Program of Central South University (Nos. 2013zzts185 and 2012zzts066). The authors would like to express their sincere thanks to Professor Marc. A. Meyers at university of California, San Diego for good suggestions and experimental conditions.

#### References

- [1] C. Zener, J.H. Hollomon, *J. Appl. Phys.* 15 (1944) 22–32.
- [2] B. Dodd, Y.L. Bai, *Adiabatic Shear Localization: Frontiers and Advances*, second ed., Elsevier Science Ltd, London, 2012.
- [3] M.A. Meyers, Y.B. Xu, Q. Xue, M.T. Perez-Prado, T.R. McNelley, *Acta Mater.* 51 (2003) 1307–1325.
- [4] B.K. Kad, J.M. Gebert, M.T. Pérez-Prado, M.E. Kissner, M.A. Meyers, *Acta Mater.* 54 (2006) 4111–4127.
- [5] C.Z. Duan, M.J. Wang, *J. Mater. Process. Technol.* 168 (2005) 102–106.
- [6] K.M. Cho, S. Lee, S.R. Nutt, *Acta Metall.* 41 (1993) 923–932.
- [7] M.A. Meyers, G. Subhash, B.K. Kad, L. Prasad, *Mech. Mater.* 17 (1994) 175–193.
- [8] Q. Xue, J.F. Bingert, B.L. Henrie, G.T. Gray III, *Mater. Sci. Eng. A* 473 (2008) 279–289.
- [9] C.Z. Duan, Y.J. Cai, M.J. Wang, *J. Mater. Sci.* 44 (2009) 897–902.
- [10] S.K. Dhua, P.P. Sarkar, *Mater. Sci. Eng. A* 575 (2013) 177–188.
- [11] K.M. Lee, H.C. Lee, *J. Mater. Process. Technol.* 210 (2010) 1574–1579.
- [12] X.P. Ma, L.J. Wang, C.M. Liu, S.V. Subramanian, *Mater. Sci. Eng. A* 539 (2012) 271–279.
- [13] B.F. Wang, Z.L. Liu, J. Li, *Mater. Sci. Eng. A* 568 (2013) 20–24.
- [14] L.W. Meyer, S. Manwarling, in: L.E. Murr, K.P. Staudhammer, M.A. Meyers (Eds.), *Metallurgical Applications of Shock-Wave and High-Strain-Rate Phenomena*, Marcel Dekker, New York, 1986, pp. 657–674.
- [15] U. Andrade, M.A. Meyers, K.S. Vecchio, A.H. Chokshi, *Acta Metall. Mater.* 42 (1994) 3183–3195.
- [16] R.S. Culver, in: R.W. Rohde, B.M. Butcher, J.R. Holland (Eds.), *Metallurgical Effects at High Strain Rates*, Plenum Press, New York, 1973, pp. 519–530.
- [17] Y. Zou, W. Qin, E. Irissou, J.G. Legoux, S. Yue, J.A. Szpunar, *Scr. Mater.* 61 (2009) 899–902.
- [18] Y. Yang, X.M. Zhang, Z.H. Li, Q.Y. Li, *Acta Mater.* 44 (1996) 561–565.
- [19] Q. Xue, G.T. Gray, B.L. Henrie, S.A. Maloy, S.R. Chen, *Metall. Mater. Trans. 36A* (2005) 1471–1486.
- [20] S. Nemat-Nasser, J.B. Isaacs, M. Liu, *Acta Mater.* 46 (1998) 1307–1325.
- [21] C.A. Bronkhorst, E.J. Cerreta, Q. Xue, P.J. Maudlin, T.A. Mason, G.T. Gray III, *Int. J. Plasticity* 22 (2006) 1304–1335.
- [22] V.F. Nesterenko, M.A. Meyers, J.C. Lasalvia, M.P. Bondar, Y.J. Chen, Y. L. Lukyanov, *Mater. Sci. Eng. A229* (1997) 23–41.
- [23] V.F. Nesterenko, M.A. Meyers, T.W. Wright, *Acta Mater.* 46 (1998) 327–340.

- [24] M.A. Meyers, V.F. Nesterenko, J.C. Lasalvia, Q. Xue, *Mater. Sci. Eng. A* 317 (2001) 204–225.
- [25] P.R. Guduru, A.J. Rosakis, G. Ravichandran, *Mech. Mater.* 33 (2001) 371–402.
- [26] S.F. Li, W.K. Liu, D. Qian, P.R. Guduru, A.J. Rosakis, *Comput. Methods Appl. Mech. Eng.* 191 (2001) 73–92.
- [27] Y. Yang, B.F. Wang, J. Xiong, X.Y. Yang, Y. Zeng, Z.P. Chen, *Metall. Mater. Trans. A* 37 (2006) 3131–3137.
- [28] H. Hu, B. Rath, *Metall. Trans. 1* (1970) 3181–3184.
- [29] Z. Zhang, C. Wu, *Comput. Mater. Sci.* 65 (2012) 442–449.